

Strong magnon-photon coupling in on-chip CoFe/$LiNbO_3$ hybrid nanostructures

Jinlong Wang(王锦龙), Rundong Yuan(袁润东), Manuel Mueller, Luis Flacke, Hanchen Wang(王涵晨), Kanglin Yu(俞康麟), Junfeng Hu(胡俊峰), Fenglin Zhong(钟丰麟), Jilei Chen(陈济雷), Mathias Weiler, Matthias Althammer, and Haiming Yu(于海明)

Citation: Chin. Phys. B, 2026, 35 (**4**): 047503. DOI: 10.1088/1674-1056/ae2d3c
http://cpb.iphy.ac.cn; http://iopscience.iop.org/cpb

What follows is a list of articles you may be interested in

Dissipative-coupling-induced magnomechanical chaos

Qin Wu(吴琴), Jiao Peng(彭椒), Yu-Dong Chen(陈毓东), and Zeng-Xing Liu(刘增星)
Chin. Phys. B, 2026, 35 (**3**): 037501. DOI: 10.1088/1674-1056/adfa7a

Controlling coupled magnons with pumps

Fan Yang(杨帆), Chenxiao Wang(王辰笑), Zhijian Chen(陈志坚), Kaixin Zhao(赵恺欣), Weihao Liu(刘炜豪), Shuhuan Ma(马舒寰), Chunke Wei(魏纯可), Jiantao Song(宋剑涛), Jinwei Rao(饶金威), and Bimu Yao(姚碧霖)
Chin. Phys. B, 2025, 34 (**10**): 107508. DOI: 10.1088/1674-1056/addce3

Temperature and angle dependence of magnetic damping in manganite thin films

Jinghua Ren(任京华), Yuelin Zhang(张跃林), Miming Cai(蔡米铭), Yuhan Li(李语涵), Mingming Li(李明明), Tianqi Wang(王天琦), Dekun Shen(沈德坤), Hongyu Zhou(周鸿渝), Xiangwei Zhu(朱祥维), and Jinxing Zhang(张金星)
Chin. Phys. B, 2025, 34 (**10**): 107504. DOI: 10.1088/1674-1056/ade06d

Bifurcation of the bound states in the continuum in a dissipative cavity magnonic system

Xinlin Mi(米锌林), Lijun Yan(闫丽君), Bimu Yao(姚碧霖), Shishen Yan(颜世申), Jinwei Rao(饶金威), and Lihui Bai(柏利慧)
Chin. Phys. B, 2025, 34 (**6**): 067508. DOI: 10.1088/1674-1056/add4e4

Frequency combs based on magnon-skyrmion interaction in magnetic nanotubes

Tijjani Abdulrazak, Xuejuan Liu(刘雪娟), Zhejunyu Jin(金哲珺雨), Yunshan Cao(曹云姗), and Peng Yan(严鹏)
Chin. Phys. B, 2024, 33 (**8**): 087503. DOI: 10.1088/1674-1056/ad4ff5

SPECIAL TOPIC — Advanced magnonics

Strong magnon–photon coupling in on-chip CoFe/$LiNbO_3$ hybrid nanostructures

Jinlong Wang(王锦龙)[1,2,†], Rundong Yuan(袁润东)[3,†], Manuel Mueller[4,5], Luis Flacke[4,5], Hanchen Wang(王涵晨)[6], Kanglin Yu(俞康麟)[1,2], Junfeng Hu(胡俊峰)[1], Fenglin Zhong(钟丰麟)[7], Jilei Chen(陈济雷)[1], Mathias Weiler[8], Matthias Althammer[4,5,‡], and Haiming Yu(于海明)[1,2,§]

[1] *International Quantum Academy, Shenzhen* 518048, *China*
[2] *Fert Beijing Institute, MIIT Key Laboratory of Spintronics, School of Integrated Circuit Science and Engineering, Beihang University, Beijing* 100191, *China*
[3] *TCM Group, Cavendish Laboratory, University of Cambridge, J. J. Thomson Avenue, Cambridge CB*3 0*HE, United Kingdom*
[4] *Walther-Meißner-Institut, Bayerische Akademie der Wissenschaften, Garching* 85748, *Germany*
[5] *TUM School of Natural Sciences, Technical University of Munich, Garching* 85748, *Germany*
[6] *Department of Materials, ETH Zurich, Zurich* 8093, *Switzerland*
[7] *CDT in Superconductivity, Cavendish Laboratory, University of Cambridge, J. J. Thomson Avenue, Cambridge CB*3 0*HE, United Kingdom*
[8] *Fachbereich Physik and Landesforschungszentrum OPTIMAS, Technische Universität Kaiserslautern, Kaiserslautern* 67663, *Germany*

(Received 10 November 2025; revised manuscript received 12 December 2025; accepted manuscript online 16 December 2025)

We demonstrate strong magnon–photon coupling using on-chip arrays of ferromagnetic CoFe nanowires fabricated on a dielectric lithium niobate substrate. A large coupling strength of 1.1 GHz and a cooperativity of 3.1 at a frequency of 24.5 GHz are achieved in CoFe nanowires with a volume of 110 μm^3, facilitated by the enhanced spin–photon interaction at the single-spin level. The measured spectra are analyzed using a semiclassical theoretical model that combines the Landau–Lifshitz equation with Maxwell's equations. Our results provide an on-chip approach to integrated hybrid magnonics based on nanomagnets, offering promising routes for the development of coherent information-processing devices.

Keywords: magnonics, magnon–photon coupling, nanomagnet, on-chip

PACS: 75.78.–n, 76.50.+g, 52.35.Mw, 71.36.+c

DOI: 10.1088/1674-1056/ae2d3c **CSTR:** 32038.14.CPB.ae2d3c

1. Introduction

Hybrid systems that couple different quantum systems for complementary functionality have recently attracted great attention due to their advantages in quantum information processing.[1–3] One of the rapidly growing subfields in hybrid systems is hybrid magnonics,[1,4–13] where information is processed by the coherent interaction between magnons, the quanta of spin-wave excitations,[14–19] and other forms of information carriers such as microwave photons,[3–5] phonons,[20–22] magnons themselves,[23–25] and superconducting qubits.[26–30] Research on magnon–photon coupling began with spin ensembles interacting with microwave photons.[31] A pioneering experimental demonstration of coherent coupling was achieved by inserting a submillimeter-sized yttrium iron garnet into a high-quality 3D microwave cavity at room temperature.[4] Subsequently, coupled magnon–microwave photon systems have greatly developed due to their potential to realize strong light–matter coupling.[32–35] The coupling strength $g = g_s\sqrt{N}$ is typically enhanced by increasing the total number of spins N, to overcome the weak coupling strength g_s between a single spin and the microwave photon.[4,36] For this reason, most works in this area have focused on materials with macroscopic dimensions on the order of millimeters or centimeters to maximize N.

Significant progress has been made in controlling magnonic quantum states using millimeter-scale hybrid systems, enabling novel applications such as coherent microwave sources,[37] microwave–optical transducers,[38] and dark matter detection.[39] However, the large dimensions of these systems raise a critical challenge for their compatibility with modern on-chip platforms, which require planar geometry and miniaturization. To address this issue, research is increasingly shifting toward nanomagnets,[28,29] which are expected to extend the functionality of existing hybrid systems and potentially unlock new applications.[40–43] Among the promising material candidates, metallic ferromagnets such as $Co_{25}Fe_{75}$ (CoFe) have attracted growing interest. With its low Gilbert damping leading to reduced dissipation and high saturation magnetization that supports high spin density, CoFe presents a compelling pathway for developing scalable, planar devices

[†]These authors contributed equally to this work.
[‡]Corresponding author. E-mail: matthias.althammer@wmi.badw.de
[§]Corresponding author. E-mail: haiming.yu@buaa.edu.cn

© 2026 Chinese Physical Society and IOP Publishing Ltd. All rights, including for text and data mining, AI training, and similar technologies, are reserved.

compatible with integrated-circuit technology.[44–47]

In this work, we experimentally demonstrate the realization of strong coupling between magnons and photons using CoFe nanowires directly fabricated on top of a lithium niobate (LNO) planar resonator. An anticrossing gap with a magnitude of 2.2 GHz near 24.5 GHz is observed. The coupling strength g is accounted for by combining the Landau–Lifshitz equation with Maxwell's equations, which is expected to be further enhanced by optimizing the nanowires' width to maximize the stray field while maintaining a substantial number of spins N.

2. Experimental details

We expose an array of 25 identical nanowires, each with a length of 100 μm and a width $w = 1.4$ μm, spaced 200 nm apart, on a c-plane 500-μm-thick single-crystal LNO substrate using electron-beam lithography. A multilayer stack of Pt (3 nm)/Cu (3 nm)/CoFe (35 nm)/Cu (3 nm)/Ta (2 nm) is subsequently deposited via sputtering and a lift-off process to form the nanowire structures, as illustrated in Fig. 1(a). The magnetic properties of an unstructured CoFe film, including a saturation magnetization $\mu_0 M_S = 2.3$ T and an intrinsic Gilbert damping parameter $\alpha = 7.2 \times 10^{-3}$, are provided in the supplementary material.

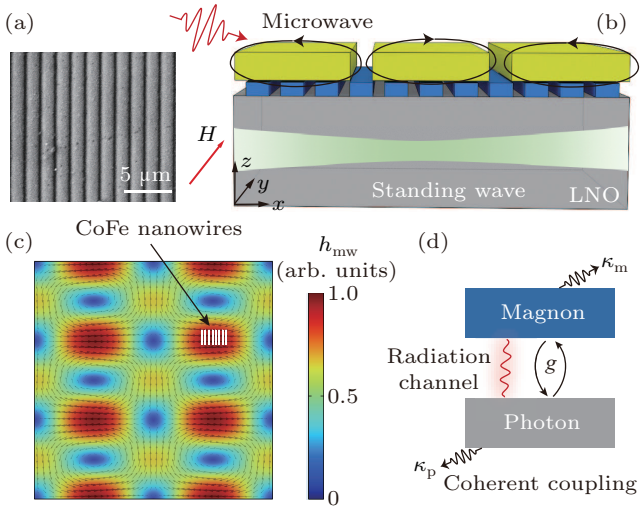


Fig. 1. (a) Scanning electron microscope (SEM) image (scale bar: 5 μm) of the CoFe nanowire array on a $LiNbO_3$ cavity. (b) Schematic of the hybrid CoFe/$LiNbO_3$ nanostructure with integrated CPWs. The external magnetic field μH is applied along the y direction, parallel to the nanowires' long axis. (c) Simulated magnetic field distribution of the cavity mode at 24.5 GHz. Arrows and color represent the field orientation and amplitude, respectively. The CoFe nanowires (white short lines) are schematically overlaid, scaled up by ten for visibility. (d) Diagram of the linearly coupled magnon–photon system, where g, κ_m, and κ_p denote the coupling strength, magnon dissipation rate, and cavity photon dissipation rate, respectively.

To excite and detect microwave signals, coplanar waveguides (CPWs) are integrated above the CoFe nanowires (Fig. 1(b)). The signal and ground lines of the CPWs have a width of 10 μm, separated by a gap of 10 μm. Microwave current in the GHz range is injected into the antenna through probe connectors linked to a vector network analyzer. The reflection response is characterized by measuring the scattering parameter S_{11} as a function of the microwave frequency and applied in-plane magnetic field μH.

3. Results and discussion

When microwave photons are introduced through the antenna, the LNO substrate efficiently confines the photons due to its relatively high refractive index.[48–50] The boundary conditions of the sample further restrict photon propagation, resulting in the formation of standing waves. This configuration can be regarded as an effective planar microwave cavity. As illustrated in Fig. 1(c), the spatial distribution of the cavity mode obtained from COMSOL simulation shows the magnetic field direction (arrows) and amplitude (color scale). Using a refractive index of 2.3 and an inner region of 10.0 mm × 10.0 mm, the cavity exhibits a resonant mode at $f = 24.5$ GHz. The CoFe nanowires are positioned at the antinode of the cavity mode, where the electromagnetic field amplitude is maximal. The external static magnetic field $\mu_0 H_0$ is applied along the wire axis (y direction). Under microwave excitation, the magnetization of the CoFe nanowires undergoes precession. The narrow geometry of the nanowires enhances the precession circularity and locally amplifies the dynamic stray field, leading to coupling between the magnon mode and the cavity photon mode.

The reflection spectra plotted against frequency and external magnetic field (Fig. 2(a)) reveal a distinct anti-crossing, which manifests coherent coupling between microwave photons and magnons, indicating strong interaction. The interaction lifts the degeneracy of the resonance frequencies due to strong hybridization of the two modes. Owing to the high saturation magnetization of CoFe (2.3 T), the resonance frequency is elevated, reaching ∼ 24.5 GHz under an applied field of $\mu_0 H_0 = 253$ mT (Fig. 2(b)). The coupling strength g, defined as half of the minimum frequency splitting at the anti-crossing gap, is extracted as $g/2\pi = 1.1$ GHz. This value is remarkable given the much smaller total magnetic volume of the CoFe nanowires (110 μm^3). Since the magnon–photon coupling strength g is proportional to the total number of spins N and the single-spin coupling strength g_s, we calculate $N = M_S V/[\gamma(\hbar/2)] = 2.15 \times 10^{13}$ using the gyromagnetic ratio $\gamma/(2\pi) = 28$ GHz/T. The corresponding $g_s = 239$ Hz, which is notably high.[28,29] The single-spin coupling g_s can be expressed as $g_s = g_e \mu_B \omega_r b_{rf}/\sqrt{8\hbar Z_r}$, where g_e is the g-factor, μ_B is the Bohr magneton, ω_r is the resonance frequency, b_{rf} is the amplitude of the oscillating magnetic field generated by the inductor, and Z_r is the characteristic impedance.[29] Using $Z_r = 50\ \Omega$ and $\omega_r = 24.5$ GHz, we calculate the absolute magnitude of the effective field to be $b_{rf} \sim 8.5$ nT. This substantial value confirms the strong oscillating magnetic field within the

nanowire structure. To quantify the advantage of the geometry, we performed a comparative analysis against a uniform CoFe film (see supplementary material for details). By accounting for the difference in total spin numbers, we reveal that the effective magnetic field experienced by the spins in the nanowire structure is approximately four times larger than that in the uniform film. This result demonstrates that the observed strong interaction stems from the geometric design, where the reduced width substantially enhances the single-spin coupling efficiency.

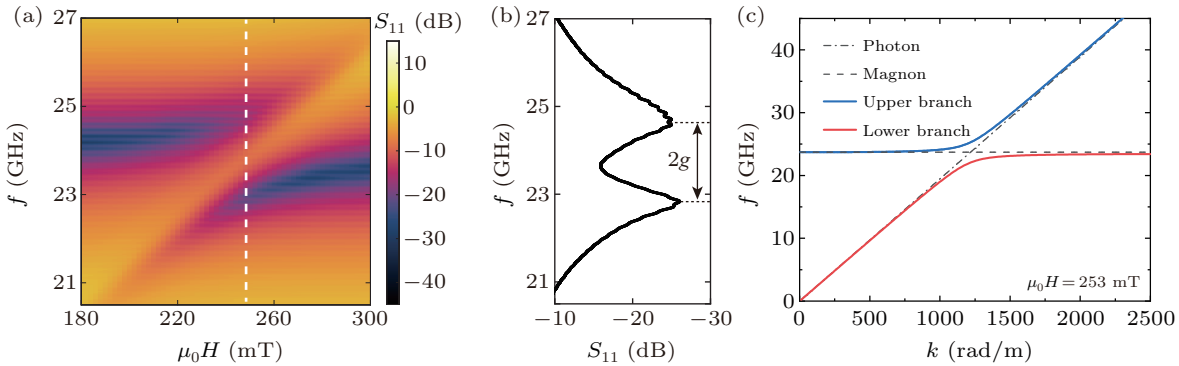


Fig. 2. (a) Microwave reflection spectra S_{11} measured as a function of frequency and in-plane magnetic field. The white dashed line indicates the field value (253 mT) at which the line cut in panel (b) is shown. A clear anti-crossing gap of 2.2 GHz is observed. (c) The theoretical coupling spectrum simulated using Eq. (1) with experimentally extracted parameters. The dash-dotted and dashed lines represent the uncoupled photon and magnon dispersions, respectively. The blue and red lines represent the magnon–polariton dispersions.

In the present device configuration, the nanoscale geometry increases the transverse demagnetization factor $N_{\rm d}$ and concurrently decreases the out-of-plane demagnetization factor N_z, which critically modifies the spin dynamics. The comparison with the unpatterned film indicates that, while the increased $N_{\rm d}$ stiffens the magnetic system and partially suppresses the dynamic magnetization, this suppression is largely offset by the change in the precession trajectory. Specifically, the orbit is corrected from a highly flattened ellipse to a nearly circular one.[51] Consequently, the enhanced dynamic dipolar fields ($h_{\rm dip}$), particularly the z-directed components, couple efficiently to the cavity field. Furthermore, the high shape anisotropy pushes the Kittel mode to the high-frequency regime, which intrinsically enhances the single-spin coupling strength. Regarding the array dynamics, the nanowires are not magnetically isolated; dipolar coupling exists between them.[52,53] This interaction reinforces the enhancement that originates from the single-wire geometric confinement. Under our broad CPW excitation ($k \approx 0$), the array does not oscillate as independent elements but rather forms a coherent quasi-uniform mode. The dipolar interaction between neighboring wires phase-locks their motion. In this collective "super-wire" state, the geometrically enhanced $h_{\rm dip}$ sums constructively across the entire array, preserving spin coherence and ultimately boosting the overall coupling strength g.

To confirm the strong-coupling regime, we determined the dissipation rates of both subsystems through the half-width at half-maximum of the respective resonances. The extracted loss rates are $\kappa_{\rm m}/(2\pi) \approx 0.41$ GHz for the magnon mode and $\kappa_{\rm p}/(2\pi) \approx 0.95$ GHz for the photon mode (see supplementary material). When the magnon mode is coupled to the photon mode, radiative damping becomes the dominant loss mechanism compared to the intrinsic magnon damping, as illustrated in Fig. 1(d). Although the cavity is not ideal and has a large dissipation rate, the system still satisfies the conditions $g > \kappa_{\rm m}$ and $g > \kappa_{\rm p}$, with a magnon–photon cooperativity $C = g^2/(\kappa_{\rm m}\kappa_{\rm p}) = 3.1$, operating in the strong-coupling regime.

The coupling mechanism in CoFe/LNO nanostructures is investigated by modeling the magnon–photon interaction with the coupled Landau–Lifshitz–Maxwell (LLM) equations. The LLM system is expressed as[54–56]

$$\begin{cases} \dfrac{\partial \boldsymbol{m}}{\partial t} = -\gamma \boldsymbol{m} \times \boldsymbol{B}_{\rm eff}, \\ \mu_0 \varepsilon \cdot \dfrac{\partial \boldsymbol{e}}{\partial t} = \nabla \times (\boldsymbol{b} + \mu_0 \beta_{\rm c} M_{\rm S} \boldsymbol{m}), \\ -\dfrac{\partial \boldsymbol{b}}{\partial t} = \nabla \times \boldsymbol{e}, \end{cases} \tag{1}$$

where $\boldsymbol{e}$ and $\boldsymbol{b}$ represent the oscillating electric and magnetic fields of the electromagnetic wave, and $\boldsymbol{m}$ is the normalized magnetic moment of the nanowires. The effective magnetic field inside the nanowires is given by $\boldsymbol{B}_{\rm eff} = \mu_0(\boldsymbol{H}_0 + \boldsymbol{H}_{\rm D}) + \boldsymbol{b}$, where $\mu_0 \boldsymbol{H}_0$ is the external bias field and $\mu_0 \boldsymbol{H}_{\rm D}$ is the demagnetizing field. $\beta_{\rm c}$ is introduced as a phenomenological scaling factor that represents the effective stray field from the nanowire magnetization that drives the cavity feedback. In our model, we assume that the dynamic stray field generated by the precessing magnetization enters the Maxwell equations and contributes to the photonic fields in LNO. Thus, $\beta_{\rm c}$ quantifies the efficiency with which the magnetization produces the coupling field $\mu_0 \beta_{\rm c} M_{\rm S} \boldsymbol{m}$, and physically $\beta_{\rm c} < 1$ is required due to the attenuation of dipolar fields. This efficiency is influenced by factors such as the nanowire geometry,

the spatial distribution of the stray fields, and the electromagnetic boundary conditions at the CoFe/LNO interface. Narrower wires enhance the precession circularity and generate a large stray field, improving its overlap with the cavity mode, while field penetration into the LNO substrate further modifies the coupling through interface boundary conditions. Because these effects are difficult to capture analytically in a simplified model, instead of solving the complex electromagnetic boundary conditions,[57,58] we use β_c as a compact parameter that incorporates their combined impact and reproduces the observed coupling strength.

Based on the established coordinate system in Fig. 1(b), we define the state vector as $\boldsymbol{\chi} = (m_x, m_z, \boldsymbol{e}^{\mathrm{T}}, \boldsymbol{h}^{\mathrm{T}})^{\mathrm{T}}$ and assume a wave-like solution $\boldsymbol{\chi} = \boldsymbol{\chi}_0 \exp[\mathrm{i}\,(\boldsymbol{k}\cdot\boldsymbol{r} - \omega t)]$. The coupled Eq. (1) can be reduced to the linear matrix form $-\mathrm{i}\omega\boldsymbol{\chi} = \boldsymbol{A}\cdot\boldsymbol{\chi}$, where the detailed components of the matrix $\boldsymbol{A}$ are provided in the supplementary material. The corresponding eigen-equation of the LLM system is given by $\| \boldsymbol{A} + \mathrm{i}\omega\boldsymbol{I}_{8\times 8} \| = 0$, in which $\boldsymbol{I}_{8\times 8}$ denotes the identity matrix. This expression can be further simplified into the polynomial form

$$\lambda_0\,\omega^6 + \lambda_1\,\omega^4 + \lambda_2\,\omega^2 + \lambda_3 = 0, \tag{2}$$

where the coefficients $\lambda_{0-3}(\boldsymbol{k})$ are also given in the supplementary material. Solving Eq. (2) at $\mu_0 H_0 = 253$ mT yields the dispersion relation $\omega(\boldsymbol{k})$ for the hybrid magnon–photon modes, which is plotted in Fig. 2(c). The calculated dispersion clearly reveals the characteristic anti-crossing gap between the magnon and photon modes.

Theoretical calculations indicate that the LNO substrate supports multiple cavity resonance frequencies, as marked by the triangles in Fig. 3(a). The magnon frequency can be tuned via an external magnetic field to match these cavity photon frequencies, as illustrated in Fig. 3(b). Although ferromagnetic resonance (FMR) magnons generally have the capability to couple with photons, the interaction remains weak when the photons in LNO are in a propagating mode rather than a confined cavity mode, due to the low photonic density of states. In contrast, when standing electromagnetic waves are established inside the cavity (marked by triangles), photons become effectively confined, leading to enhanced magnon–photon coupling. The measured coupling strengths g at the three cavity mode resonance frequencies 12.4 GHz, 16.5 GHz, and 24.5 GHz are 0.5 GHz, 0.8 GHz, and 1.1 GHz, respectively. These values increase qualitatively with the resonance frequency, consistent with the relation $g \propto g_s \propto \omega_r$. The coupling strength can be further enhanced by optimizing the cavity quality factor (to suppress dissipation), reducing the nanowire width (amplifying the dynamic dipolar field), increasing the saturation magnetization (raising the magnon frequency), and increasing the wire thickness (achieving more circular precession). As shown in Fig. 3(c), the coupling strength scales with β_c, a parameter linked to these factors. In this work, the high saturation magnetization compensates for the intentionally small β_c, suggesting that raising β_c through parameter optimization can further increase coupling, although such experimental exploration is beyond the present scope.

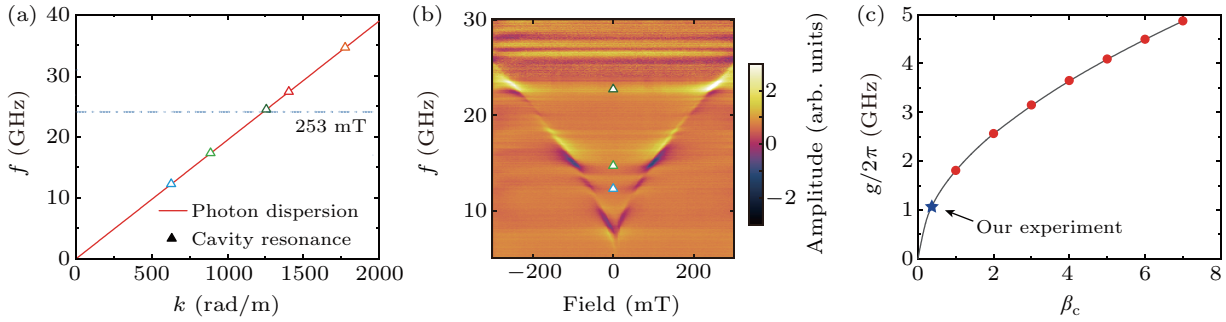


Fig. 3. (a) Relations among the FMR frequency of the CoFe nanowires at $\mu_0 H_0 = 253$ mT (blue dotted line), the cavity resonance frequencies (triangles), and the photon dispersion (red line) with refractive index $n = 2.3$. (b) Field-dependent reflection spectra of the CoFe/LNO system with the external magnetic field applied along the nanowire axis. The triangles indicate the cavity mode frequencies extracted from panel (a). (c) Magnon–photon coupling strength g as a function of the phenomenological parameter β_c.

Additionally, phonons are expected to play a significant role in this hybrid system. CoFe exhibits strong magnetoelastic properties.[59] Under microwave-driven resonance, CoFe simultaneously generates resonant phonons. Owing to the pronounced piezoelectric properties of LNO,[60,61] these phonons induce additional oscillating electric fields within the substrate, potentially enhancing the spatial overlap between the cavity electromagnetic field and the magnon mode. Future studies on magnon–photon coupling in magnetoelastic–piezoelectric heterostructures will help clarify the contribution of phonons to the coupling mechanism.

4. Conclusion

In summary, we have experimentally demonstrated strong magnon–photon coupling in CoFe/LNO ferromagnetic/dielectric nanostructures. With a single-spin–photon coupling strength $g_s = 239$ Hz, a total coupling strength of 1.1 GHz is achieved using CoFe nanowires with a volume as

small as 110 μm^3. The results are well described by a semi-classical model combining the Landau–Lifshitz and Maxwell equations. Our work establishes CoFe/LNO nanostructures as a promising platform for exploring strong magnon–photon coupling at reduced magnetic volumes. The combination of industry-compatible fabrication, large coupling strength, and high-frequency operation may open new avenues for coherent spin manipulation and quantum magnonics.

Acknowledgments

This project was supported by the National Key Research and Development Program of China (Grant No. 2022YFA1402801), the National Natural Science Foundation of China (Grant Nos. 12525406, 12474104, 12074026, and 52225106), the China Scholarship Council (CSC) Scholarship (Grant Nos. 202408060249 and 202206020091), the Cambridge Commonwealth, European, and International Trust, the Shenzhen Science and Technology Program (Grant No. RCBS20231211090814026), and the EPSRC Centre for Doctoral Training in Superconductivity (Grant No. EP/Y035453/1).

References

[1] You J Q and Nori F 2011 *Nature* **474** 589
[2] Xiang Z L, Ashhab S, You J and Nori F 2013 *Rev. Mod. Phys.* **85** 623
[3] Huebl H, Zollitsch C W, Lotze J, Hocke F, Greifenstein M, Marx A, Gross R and Goennenwein S T B 2013 *Phys. Rev. Lett.* **111** 127003
[4] Tabuchi Y, Ishino S, Ishikawa T, Yamazaki R, Usami K and Nakamura Y 2014 *Phys. Rev. Lett.* **113** 083603
[5] Zhang X, Zou C L, Jiang L and Tang H X 2014 *Phys. Rev. Lett.* **113** 156401
[6] Bai L, Harder M, Chen Y, Fan X, Xiao J and Hu C M 2015 *Phys. Rev. Lett.* **114** 227201
[7] Zhang D, Luo X Q, Wang Y P, Li T F and You J Q 2017 *Nat. Commun.* **8** 1368
[8] Jin Z J Y, Gong T C, Liu J, Yang H H, Zeng Z Z, Cao Y S and Yan P 2025 *Phys. Rev. Lett.* **135** 126702
[9] Zhang Z, Yang H, Wang Z, Cao Y and Yan P 2021 *Phys. Rev. B* **103** 104420
[10] Wang Y Q, Zhang Y, Li C Z, Wei J W, He B, Xu H J, Xia J H, Luo X M, Li J H, Dong J, He W Q, Yan Z R, Yang W L, Ma F S, Chai G Z, Yan P, Wan C H, Han X F and Yu G Q 2024 *Nat. Commun.* **15** 2077
[11] Wang Y Q, Xia J H, Wan C H, Han X F and Yu G Q 2024 *Phys. Rev. B* **109** 054416
[12] Ma K K, Li C Z, Hao Z H, Ong C K and Chai G Z 2023 *Phys. Rev. B* **109** 094422
[13] Hao Z, Yao Y, An K, Li X, Zhang C and Chai G 2025 *Phys. Rev. B* **112** 064416
[14] Kruglyak V, Demokritov S and Grundler D 2010 *J. Phys. D: Appl. Phys.* **43** 264001
[15] Lenk B, Ulrichs H, Garbs F and Munzenberg M 2011 *Phys. Rep.* **507** 107
[16] Qin H, Holländer R B, Flajšman L, Hermann F, Dreyer R, Woltersdorf G and Dijken S V 2021 *Nat. Commun.* **12** 2293
[17] Zhang Y L, Chen J L, Zhang J X and Yu H M 2022 *Appl. Phys. Rev.* **9** 041312
[18] Xu G F, An K, Ma W J, Xiling Li X L, Ong K C, Zhang C and Chai G Z 2025 *Chin. Phys. B* **34** 067507
[19] Zhang Y L, Qiu L, Chen J L, *et al.* 2025 *Nat. Mater.* **24** 69
[20] Weiler M, Huebl H, Goerg F, Czeschka F D, Gross R and Gonnenwein S T 2012 *Phys. Rev. Lett.* **108** 176601
[21] J. Zhang J, Chen M, Chen J, *et al.* 2021 *Nat. Commun.* **12** 7258
[22] Yu Z, Jin Z, Zheng Q and Yan P 2025 arXiv:2505.19673 [cond-mat.mes-hall]
[23] Qin H, Hämäläinen S J and Dijken S V 2018 *Sci. Rep.* **8** 5755
[24] Chen J, Liu C, Liu T, Xiao Y, Xia K, Bauer G E, Wu M and Yu H 2018 *Phys. Rev. Lett.* **120** 217202
[25] Li Y, Cao W, Amin V P, *et al.* 2020 *Phys. Rev. Lett.* **124** 117202
[26] Clerk A, Lehnert K, Bertet P, Petta J and Nakamura Y 2020 *Nat. Phys.* **16** 257
[27] Tabuchi Y, Ishino S, Noguchi A, Ishikawa T, Yamazaki R, Usami K and Nakamura Y 2015 *Science* **349** 405
[28] Li Y, Polakovic T, Wang Y L, et al. 2019 *Phys. Rev. Lett.* **123** 107701
[29] Hou J T and Liu L 2019 *Phys. Rev. Lett.* **123** 107702
[30] Lachance-Quirion D, Wolski S P, Tabuchi Y, Kono S, Usami K and Nakamura Y 2020 *Science* **367** 425
[31] Kubo Y, Ong F, Bertet P, *et al.* 2010 *Phys. Rev. Lett.* **105** 140502
[32] Zhang C, Shi Y, Zhang W, Jiang C and Chai G 2019 *Appl. Phys. Lett.* **115** 022407
[33] Baity P G, Bozhko D A, Macedo R, *et al.* 2021 *Appl. Phys. Lett.* **119** 033502
[34] Ma Z, Zhang Y, Guo W and Yue Z 2022 *Appl. Phys. Lett.* **121** 192401
[35] Bourcin G, Bourhill J, Vlaminck V and Castel V 2023 *Phys. Rev. B* **107** 214423
[36] Dicke R H 1954 *Phys. Rev.* **93** 99
[37] Hisatomi R, Osada A, Tabuchi Y, Ishikawa T, Noguchi A, Yamazaki R, Usami K and Nakamura Y 2016 *Phys. Rev. B* **93** 174427
[38] Yao B, Gui Y, Rao J, Zhang Y, Lu W and Hu C M 2023 *Phys. Rev. Lett.* **130** 146702
[39] Trickle T, Zhang Z and Zurek K M 2020 *Phys. Rev. Lett.* **124** 201801
[40] Dieny B, Prejbeanu I L and Garello K, et al. 2020 *Nat. Electron.* **3** 446
[41] Lisenkov I, Tyberkevych V, Levin-Pompetzki L, Bankowski E, Meitzler T, Nikitov S and Slavin A 2016 *Phys. Rev. Appl.* **5** 064005
[42] Haghshenasfard Z and Cottam M G 2020 *Phys. Rev. B* **101** 144438
[43] Gregory S G, Stenning G B, Bowden G J, Zheludev N I and Groot P A 2014 *New J. Phys.* **16** 063002
[44] Schoen M A, Thonig D, Schneider M L, Silva T, Nembach H T, Eriksson O, Karis O and Shaw J M 2016 *Nat. Phys.* **12** 839
[45] Lee A J, Brangham J T, Cheng Y, White S P, Ruane W T, Esser B D, McComb D W, Hammel P C and Yang F 2017 *Nat. Commun.* **8** 234
[46] Flacke L, Liensberger L, Althammer M, et al. 2019 *Appl. Phys. Lett.* **115** 122402
[47] Haygood I, Pufall M, Edwards E, Shaw J M and Rippard W 2021 *Phys. Rev. Appl.* **15** 054021
[48] Smith D, Riccius H and Edwin R 1976 *Opt. Commun.* **17** 332
[49] Schlarb U and Betzler K 1993 *Phys. Rev. B* **48** 15613
[50] Yu M, Barton D, Cheng R, et al. 2022 *Nature* **612** 252
[51] Wang Q, Heinz B, Verba R, Kewenig M, Pirro P, Schneider M, Meyer T, Lägel B, Dubs C, Brächer T and Chumak A V 2019 *Phys. Rev. Lett.* **22** 247202
[52] Wang Q, Pirro P, Verba R, Slavin A, Hillebrands B and Chumak A V 2018 *Sci. Adv.* **4** e1701517
[53] Wang Q, Kewenig M, Schneider M, et al. 2020 *Nat. Electron.* **3** 765
[54] Li W, Yuan R, Zhong F, Peng B, Ansermet J P and Yu H 2025 arXiv:2510.08334
[55] Jackson J D 2021 *Classical Electrodynamics* (John Wiley & Sons)
[56] Okamoto A, Shindou R and Murakami S 2020 *Phys. Rev. B* **102** 064419
[57] Yao B, Gui Y, Xiao Y, Guo H, Chen X, Lu W, Chien C and Hu C M 2015 *Phys. Rev. B* **92** 184407
[58] Bourhill J, Yu W, Vlaminck V, Bauer G E, Ruoso G and Castel V 2023 *Phys. Rev. Appl.* **19** 014030
[59] Schwienbacher D, Pernpeintner M, Liensberger L, Edwards E R, Nembach H T, Shaw J M, Weiler M, Gross R and Huebl H 2019 *J. Appl. Phys.* **126** 103902
[60] Weiler M, Dreher L, Heeg C, Huebl H, Gross R, Brandt M S and Goennenwein S T B 2011 *Phys. Rev. Lett.* **106** 117601
[61] Dreher L, Weiler M, Pernpeintner M, Huebl H, Gross R, Brandt M S and Goennenwein S T B 2012 *Phys. Rev. B* **86** 134415